THE ASTROPHYSICAL JOURNAL, 498:486–496, 1998 May 1

MATRIX-ISOLATED NANO-SIZED CARBON GRAINS AS AN ANALOG FOR THE 217.5 NANOMETER FEATURE CARRIER

M. SCHNAITER, H. MUTSCHKE, J. DORSCHNER, AND TH. HENNING
Astrophysikalisches Institut und Universitäts-Sternwarte (AIU), Friedrich-Schiller-Universität Jena, Schillergäßchen 2-3, D-07745 Jena, Germany

AND

F. SALAMA
Space Science Division, NASA Ames Research Center, Moffett Field, CA 94035-1000
Received 1997 August 12; accepted 1997 December 11

ABSTRACT

The effect of particle shape or particle clustering on the extinction behavior of nano-sized hydrogenated carbon grains is investigated experimentally. The particles were extracted by a molecular beam technique at different condensation and clustering states and isolated in an argon matrix for UV spectroscopy. The state of clustering in the samples was controlled by transmission electron microscopy analysis. The simple spherical morphology of the matrix-isolated nonagglomerated particles permitted the derivation of reliable optical constants. A clear correlation was found between the measured UV feature width and the degree of particle clustering, in agreement with theoretical investigations based on the derived optical data. Therefore, the results prove unambiguously the expectation that the optical properties of carbonaceous grain material are strongly influenced by the particle shape and the clustering degree. For particles produced in hydrogen-containing atmospheres, the UV extinction peak was shifted blueward to a position close to the 217.5 nm hump. This shift was found to be nearly independent of the amount of hydrogen in the condensation zone. We also discuss the infrared spectra of the hydrogenated carbon materials. The astrophysical implications of the results are discussed with regard to the observational as well as the elemental abundance constraints.

Subject headings: dust, extinction — ISM: abundances — line: identification — methods: laboratory — ultraviolet: ISM

1. INTRODUCTION

The 217.5 nm hump is the dominant and most controversial feature of the interstellar extinction curve. Since its discovery by Stecher (1965), it has been attributed to π-electron plasmon absorption or π-π^* band transitions in small graphite particles or amorphous carbon grains. Despite the early assignment to carbonaceous material, the exact physical nature of the carrier is still unknown.

It was first shown by Dorschner (1973) and Savage (1975) using *OAO 2* data, and later by Fitzpatrick & Massa (1986) with *IUE* data, that the interstellar extinction curve can be parameterized in the hump region by a linear background plus a Lorentz or Drude profile, respectively. Following the parameterization scheme of Fitzpatrick & Massa (1986), most of the interstellar extinction curves observed toward different lines of sight can be fitted by the simple function

$$k(\lambda) = \frac{A(\lambda) - A_V}{A_B - A_V} = a_1 + a_2\,\lambda^{-1} + \frac{a_3}{[\lambda^{-1} - (\lambda_0^{-1})^2/\lambda^{-1}]^2 + \gamma^2} \quad (1)$$

in the spectral region between 3.3 and 5.9 μm.

In equation (1), A is the magnitude of extinction, and a_1 and a_2 are fitting parameters describing the linear background. The parameter a_3 describes the strength of the Drude absorption profile at position λ_0 and with width γ. This mathematical description of the hump region, giving only hints as to the physical nature of the carrier, is helpful in identifying and quantifying correlations between the hump parameters and variations in the interstellar environment. The main observational constraints, which have been unraveled from such systematic investigations of the hump region along different lines of sight, are the remarkable constancy of the peak position, $\lambda_0^{-1} = 4.60\ \mu\mathrm{m}^{-1}$ (variations $\leq 1\%$), and large variations in the peak width γ around a mean value of $1.0\ \mu\mathrm{m}^{-1}$ (variations $\leq 25\%$). The latter are mainly uncorrelated with the weak variations in the peak position (Fitzpatrick & Massa 1986; Jenniskens & Greenberg 1993). For larger wavenumbers ($5.9 < \lambda^{-1} < 8.0\ \mu\mathrm{m}^{-1}$), the extinction curve can be parameterized by adding a nonlinear rise to the short-wavelength extrapolation of the linear component in the hump region. The shape of the nonlinear rise is almost the same for all lines of sight, and its strength is uncorrelated with the underlying linear component, while there are weak correlations with the hump height and width (Jenniskens & Greenberg 1993).

Physical models of cosmic dust rely on optical properties measured carefully for specific analog materials available in the laboratory. Their relevance is a function of their compatibility with observational and cosmic abundance constraints. One approach is to use bulk optical data as an input in the calculation of small-particle optical properties. For these calculations, a reasonable model of the morphology of the cosmic grains must be used. In this theoretical approach, graphite is by far the most frequently adopted candidate for the hump carrier; it is included in the form of small ($a \leq 20$ nm) spheroidal grains in various dust models that reproduce the interstellar extinction curve (Mathis, Rumpl, & Nordsieck 1977; Hong & Greenberg 1980; Draine & Lee 1984; Mathis 1996). A new "unified" model by Li & Greenberg (1997) also refers to the optical data of graphite without explicitly naming the hump carrier. However, in order to satisfy the observational constraints, especially the peak position, the dielectric function of graphite has been modified in most of the models. Mantles

around the graphite grains have been proposed to explain the observed variation in bandwidth. Recently, Rouleau, Henning, & Stognienko (1997) have shown that small compact clusters composed of spherical graphite particles with a slightly modified dielectric function produce a very stable peak position, while the feature width varies in a wide range.

This theoretical approach has the shortcoming that graphite is a highly anisotropic, crystalline material and therefore will hardly be found in the form of spherical or spheroidal particles in nature. Real carbonaceous dust grains produced in laboratories or found in meteorites are disordered. Therefore, to complement the theoretical approach using a tailored dielectric function and an ideal morphology it is important to directly measure the extinction properties of small carbonaceous grains produced under astrophysically related conditions in the laboratory (Colangeli et al. 1995; Mennella et al. 1995a; Jäger et al. 1998).

Such realistic carbonaceous grains show a great structural variety, owing to the three possible hybridization states (sp^1, sp^2, and sp^3) of carbon and additional mixed hybrids (e.g., "fullerene-like") that carbon atoms can adopt in chemical bonds. These different hybrids, present in variable concentration and in a heterogeneous arrangement, form the chemical bonding skeleton of the grains. The use of the term "amorphous" for this type of solid-state structure is misleading, since a medium-range order is often present to some extent in the form of "graphitic units," i.e., stacked aromatic layers with sizes on the order of 10 Å. Furthermore, recent high-resolution transmission electron microscopy (HRTEM) analyses have shown that bent layered graphitic structures must also be taken into account when discussing the structures of such carbonaceous materials (Jäger et al. 1998). Since in these semiconducting carbonaceous solids the π electrons produce the electronic density of states near the Fermi energy, the sp^2-bonded or graphitic substructures determine the optical gap. Interband transitions between the binding and antibinding π electron bands occur mainly in the UV, with a maximum between 200 and 260 nm, whereas those of the σ electrons are located around 80 nm.

Much experimental work has been done in order to derive the relationship between the internal structure and the optical absorption characteristics of carbon grains and carbon thin films (for a review see Papoular et al. 1996). The UV spectra obtained so far in these studies generally show absorption features in the spectral region of the π electron transitions that are too broad compared to the interstellar UV feature. Following Huffman (1988), this behavior has usually been ascribed to clustering of the grains. In fact, for most of the collected carbon grain samples, a heavily coagulated, chainlike cluster morphology is observed (Colangeli et al. 1995), which strongly influences the infrared absorption (Rouleau & Martin 1991; Stognienko, Henning, & Ossenkopf 1995) and could also be crucial for the UV optical properties of these carbon particles.

It is well known from Mie theory that for spheres of small size compared to the wavelength of light ($2\pi a/\lambda \ll 1$), surface resonances (Fröhlich modes) are predicted in spectral regions of strong absorption of the grain material (Bohren & Huffman 1983). As a consequence, these absorption bands become stronger and narrower, and for small isolated spheres are blueshifted compared to the bulk features. For arbitrarily shaped particles or for clusters of particles, this effect is reduced depending on the shape distribution and the state of clustering. For realistic grain morphologies, an exact calculation of absorption cross sections in these spectral regions of strong absorption is not available. However, it has recently become possible to exactly calculate the extinction caused by aggregates of touching spheres (Rouleau 1996). The results of such calculations carried out with the optical data for graphite confirm the significance of clustering effects for the UV extinction by carbon grains (Rouleau et al. 1997).

It has been a long-standing open question whether the dielectric function representing the UV optical properties of amorphous carbon grains fulfills the Fröhlich conditions for the occurrence of surface resonances in the spectral region of the π-π^* transition. The optical data available so far for amorphous carbon materials show huge differences, mainly because of large variations in the internal structures. Most of these data have been derived for amorphous carbon films or glassy carbon. A number of authors (Rouleau & Martin 1991; Preibisch et al. 1993; Zubko et al. 1997) have also extracted optical data from carbon grain spectra. However, these studies suffer from the necessity of modeling the complicated grain morphology by a relatively simple geometry (e.g., a continuous distribution of ellipsoidal grains). The reliability of the results cannot be proven, as independent accurate optical data are not available for this material.

The only way to overcome these many problems is to measure the absorption characteristics of isolated nonagglomerated carbon grains. Since these grains (often designated as primary particles in this paper) are roughly spherical, such a measurement would enable us to derive the optical data of the material by an exact calculation. If shape effects are indeed important, the UV absorption spectrum should show a sharpened π-π^* transition feature that may be much closer to the interstellar feature.

For that purpose we have developed a new experimental technique consisting of the extraction of primary carbon grains from different sources (flames, bulk evaporation) by a free-jet expansion, and the subsequent isolation of these particles in noble gas solid matrices for in situ spectroscopic analysis. Preliminary experiments with small carbon grains ($a \approx 3$ nm) produced in low-pressure acetylene/oxygen flames have shown that the π-π^* absorption profile varies strongly with the degree of clustering (Schnaiter et al. 1996).

In this paper, we present an investigation of the optical properties of matrix-isolated single and clustered nanosized (hydrogenated) carbon grains that have been prepared by condensation of resistively vaporized graphite electrode material in a quenching gas. The experimental setup is described in § 2. The results for particle samples with varying clustering degrees are compared in § 3.1 with experimental and theoretical results found in the literature and with our own theoretical investigations. In § 3.2, the results found for isolated primary grains produced in hydrogen-containing quenching gases are presented. In § 4, the implications of our results for interstellar dust models are discussed through a comparison with the 217.5 nm hump of the mean interstellar extinction curve. The amount of carbon required to produce the observed UV hump based on our laboratory material is derived and compared with the latest determinations of the cosmic carbon abundance.

2. EXPERIMENTAL SETUP

The device we use combines two experimental techniques that are well established in molecular physics and cluster physics, namely, matrix-isolation spectroscopy and the molecular beam technique. The matrix-isolation technique is usually applied to store unstable ions and radicals isolated from each other in an inert matrix for subsequent investigation of their molecular properties by spectroscopic methods (Andrews & Moskovits 1989). Therefore, matrix isolation can be regarded as an approximation for isolated particles in the gas phase, with the restriction that the matrix always interacts with the trapped species in such a way that the spectral signatures are shifted unsystematically, depending on the matrix material, the activated transition mode, and the trapping site (Barnes 1981). In the case of trapped solid particles with huge sizes compared to the atomic distances in the matrix, the situation is much simpler. Here, local interactions between the nearest matrix atoms and the trapped species lose their importance, and the matrix acts as a homogeneous medium with a real refractive index n (Schnaiter et al. 1996).

The experimental setup is sketched in Figure 1. In the source chamber, graphite rods are resistively heated to the sublimation temperature. The generated carbon vapor is quenched in a cooling gas atmosphere (argon/hydrogen at 10 mbar) to form small solid grains. The impurity of the cooling gas is about 1 ppm. The cooling-gas pressure is controlled electronically by means of a flow meter in combination with a gas-independent gauge and is held constant with an accuracy of 1%. The quenching gas expands through a nozzle (orifice 0.8 mm) into a second chamber pumped separately to a pressure of about 10^{-3} mbar. As a result of the drop in pressure during expansion, the particles are decoupled from the gas and further particle growth is stopped. A sharp-edged skimmer peels a particle beam out of the free jet into a third chamber, maintained at a pressure of about 10^{-5} mbar. A sample holder is located in this chamber to collect the particles from the beam for transmission electron microscopy (TEM) analysis. A cold CaF_2 substrate (maintained at 14 K) is mounted in such a way that it can rotate in a fourth chamber at a pressure of about 10^{-7} mbar. The substrate covers half of the beam cross section. The other half is used to monitor the mass rate by a (quartz) microbalance. The beam particles that reach the cold surface of the substrate are isolated in a growing solid argon matrix. For the interpretation of the measured spectra as single-particle spectra, the distances between the particles are required to be much larger than their dimensions. This condition is expressed in terms of the volume fraction $f = V_{par}/V_{tot}$, where V_{par} is the entire volume of the embedded particles and V_{tot} is the total volume of the sample. Volume ratios of $f \leq 1\%$ are recommended and were adjusted during the preparation of the matrix-isolated samples by controlling the matrix growth as well as the particle mass rate. For each sample, a pure Ar matrix is generated on the substrate for reference and to control the thickness of the matrix by shutting a part of the beam with a diaphragm. After the isolation of a sufficient quantity of particles in the matrix, UV-VIS spectroscopy is performed in transmission after rotating the cold substrate into the spectrometer beam. The UV-VIS spectrometer used (Zeiss Specord S5) covers the wavelength region between 200 and 620 nm, with a practical resolution of about 2.4 nm.

Infrared spectroscopy was performed on the hydrogenated carbon samples in the wavelength range between 2 and 20 μm, with a resolution of 1 cm^{-1}. For these measurements an FTIR spectrometer (Bruker 113v) was used.

3. RESULTS

Two series of samples were prepared and analyzed. The first set of samples were formed with constant cooling-gas conditions (pure argon at 10 mbar), but at varying distances

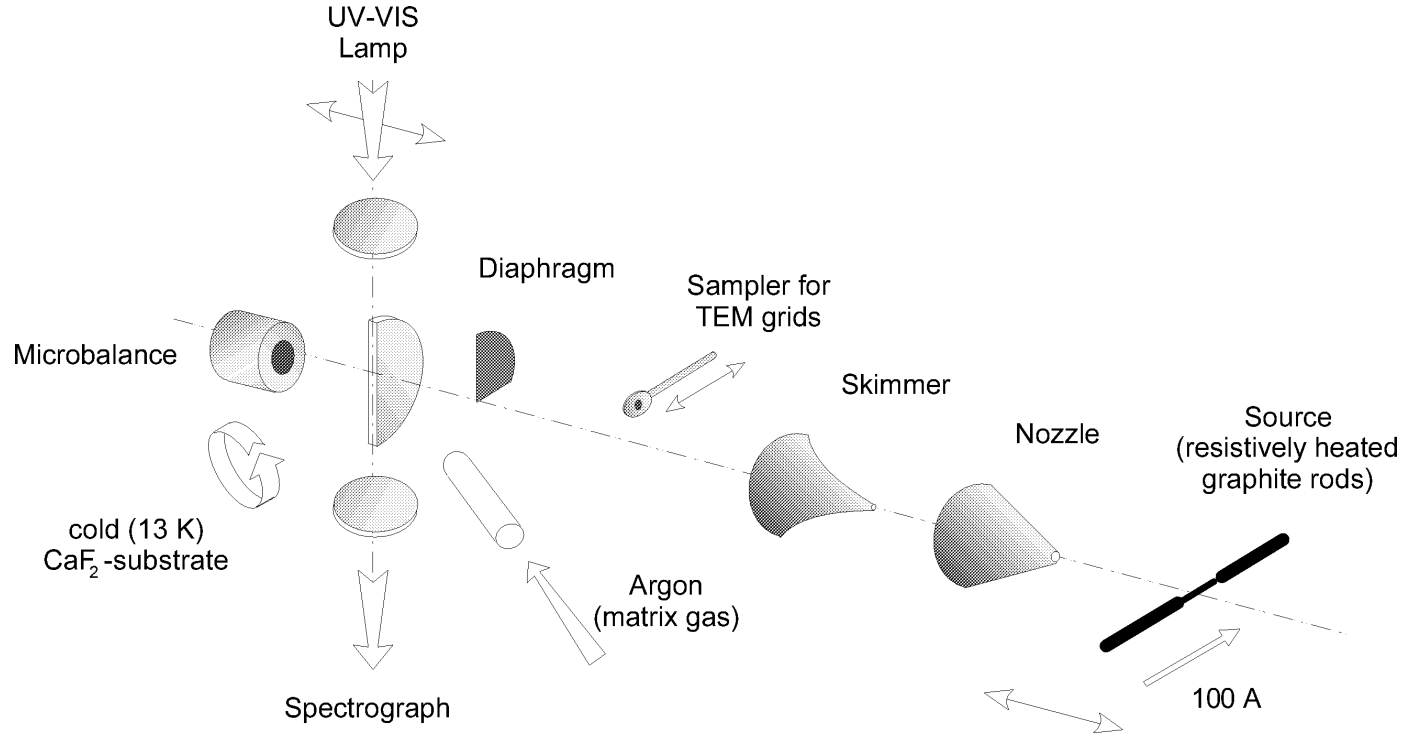

FIG. 1.—Experimental setup

between the source and the extraction nozzle. Such a procedure enables the spectroscopic analysis of isolated particles and clusters at different growth and coagulation states. A second sample series was performed at a constant short extraction distance but with a varying amount of hydrogen in the quenching gas. In this case, the effect of hydrogen incorporation on the optical behavior of the primary condensed nano-sized grains could be investigated without the disturbing effect of particle clustering.

3.1. *The Effect of Particle Clustering*

To study the influence of particle coagulation on their extinction behavior, particle samples were prepared in a pure Ar atmosphere at three distinct distances (15, 20, and 25 mm) between the extraction nozzle and the source. For each extraction distance, samples were collected from the beam for TEM analysis, in order to obtain information about the particle morphology for each of the distinct condensation and growth zones in the source.

Figure 2 shows representative examples of the TEM results. The grains extracted at 15 mm from the evaporation source are isolated small primary particles with diameters of about 5–15 nm (Fig. 2*a*). At an extraction distance of 25 mm, the beam is dominated by small clusters composed of a few to about 50 primary particles (Fig. 2*b*). The correlation of the clustering state of the sample with the extraction distance has been reproduced in a number of experimental runs. Obviously, clustering takes place outside an inner growth zone, the radius of which (here about 15 mm) varies with the type of cooling gas, the pressure, and probably with the evaporation rate. We kept the evaporation rate more or less constant by measuring the particle mass flow with the microbalance and controlling the heating current. We also checked by high-resolution transmission electron microscopy (HRTEM) that the internal structure of the extracted particles did not change with the extraction distance.

The normalized absorption curves for the samples of Figures 2*a* and 2*b*, isolated in solid argon, are plotted in Figure 3*a*. The spectra show a systematic broadening of the π-π^* absorption feature that is obviously correlated with the increase of clustering in the samples. The peak position

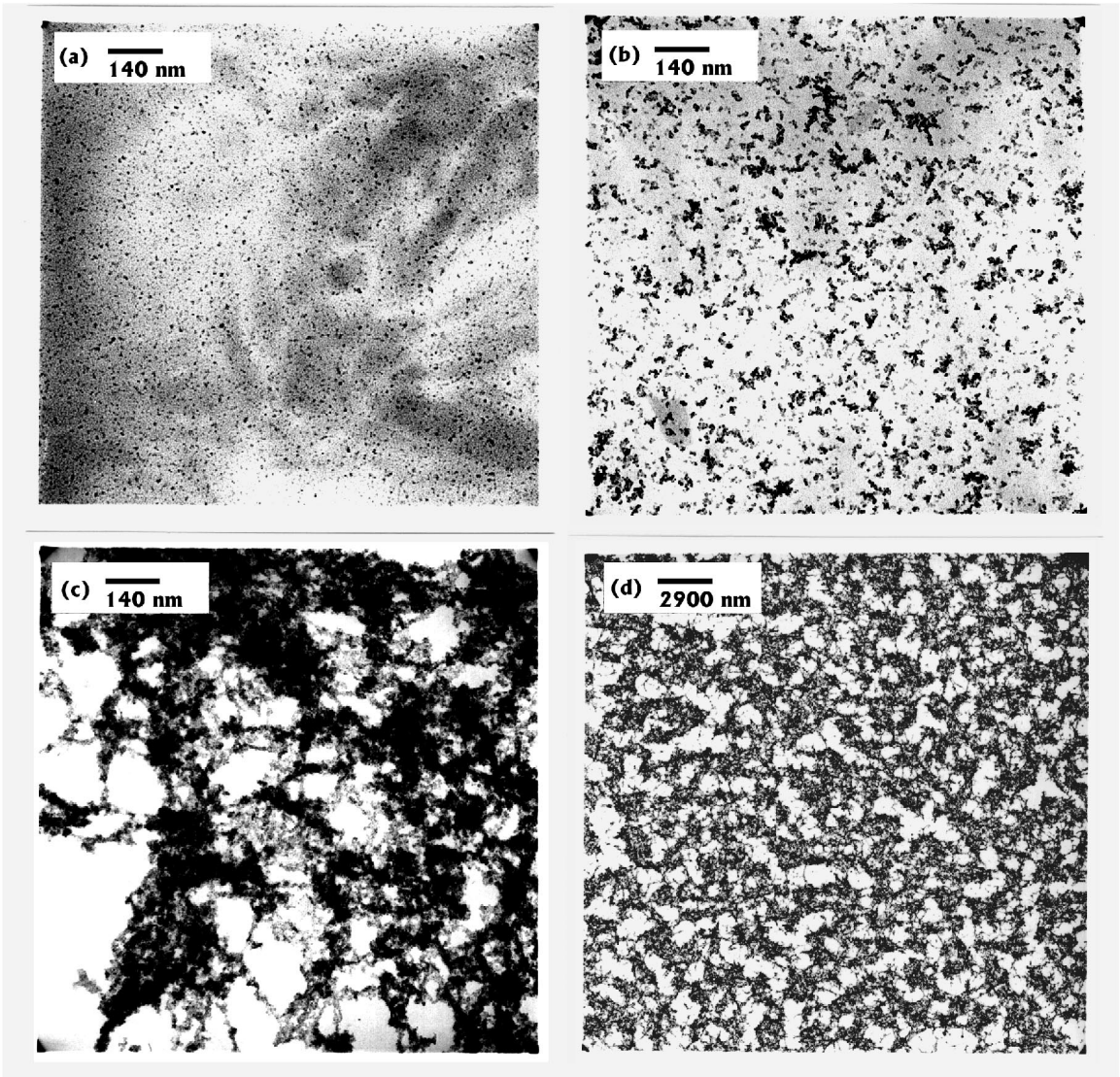

FIG. 2.—*Upper panels*: TEM images of carbon grains collected from the beam at an extraction distance of (*a*) 15 mm and (*b*) 25 mm relative to the source. *Lower panels*: TEM images of the residue left on the substrate after the evaporation of the matrix, (*c*) at the same magnification as in the upper part, and (*d*) at a lower magnification to show the long-range structure in these residues.

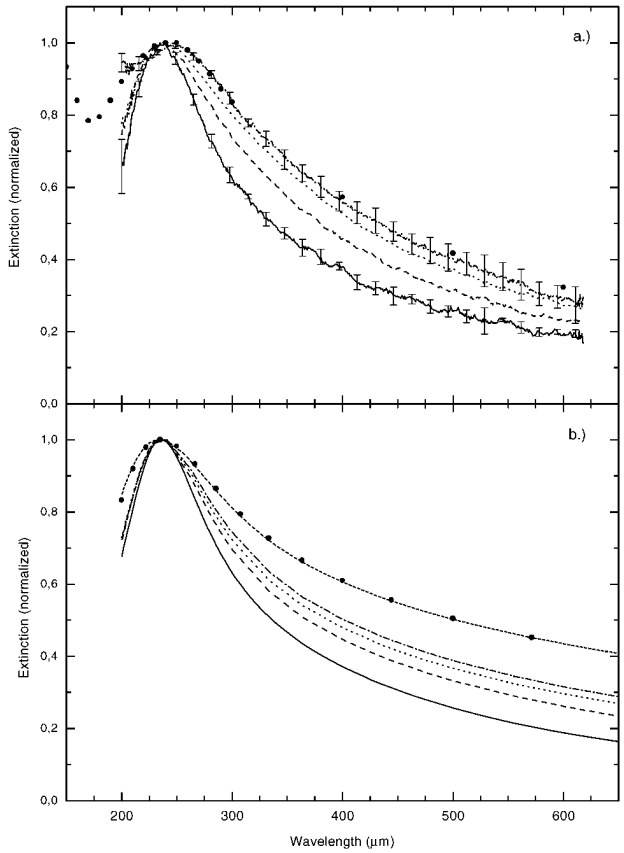

FIG. 3.—(*a*) UV-VIS absorption spectra of carbon grains extracted at different distances and isolated in solid argon at 14 K for 15 mm (AR15; *solid line*), 20 mm (AR20; *dashed line*), and 25 mm (AR25; *dotted line*). The spectrum of the 15 mm sample after evaporation of the matrix is also plotted (AR15RE; *dash-dotted line*). This accurately fits the ACAR spectrum reported by Colangeli et al. (1995) (*solid circles*). (*b*) Calculations using the optical data derived from the AR15 spectrum of (*a*) for a single Rayleigh sphere (*solid line*), and for $N = 4$ (*dashed line*), $N = 16$ (*dotted line*), and $N = 32$ (*dash-dotted line*) CCA clusters. To simulate the spectrum of the strongly coagulated AR15RE sample in (*a*), the results of a CDE calculation in vacuum (*short-dashed line*) and of an EMT with a filling factor of 0.25 between carbon and vacuum (*solid circles*) are also plotted.

is quite stable, in qualitative agreement with the results of Rouleau et al. (1997) for small clusters of graphite spheres. The TEM analysis indicates that the spectrum of the sample extracted at 15 mm (designated as AR15 in Fig. 3*a*) is the UV absorption spectrum of a collection of isolated, small, spherical amorphous carbon grains. The spectrum of a layer of clustered amorphous carbon particles collected from an arc discharge (in Ar at 10 mbar) on a substrate without a matrix (Colangeli et al. 1995; ACAR sample) is also shown for comparison in Figure 3*a*.

The ideal morphology of the AR15 sample has enabled us to derive the optical constants of the particle material by an exact calculation using the absorption cross section of Rayleigh spheres isolated in a solid argon matrix with a real refractive index of $n = 1.29$ (Schulze & Kolb 1973). The dielectric function of the amorphous carbon material was modeled by only two Lorentz oscillators, giving a nearly exact representation of the absorption profile. One of these represents the π-absorption band, the other a very broad, nearly constant absorption background. The real part of the dielectric function in the short-wavelength limit necessary for this kind of model was taken to be $\epsilon_0' = 2.5$, from a fit of the σ-σ^* band in the dielectric function of glassy carbon (Edoh 1983). The resulting optical data are plotted in Figure 4, together with the optical data derived by a similar fitting procedure from the spectrum of a hydrogenated carbon grain sample (H50, see § 3.2), the "artificial cosmic graphite" data for an electric field perpendicular to the graphite *c*-axis derived by Draine & Lee (1984), and with the recently published optical data extracted from the clustered ACAR grain spectrum (depicted in Figure 3*a*) by Zubko et al. (1997). To simulate the measured change of the UV feature width as a function of the clustering degree in the sample, we used the generalized Mie code developed by Rouleau (1996) to calculate the extinction of small cluster-cluster agglomerates (CCA) based on the optical data derived for our system (AR15). For small clusters, the CCA cluster configuration is not very different from the particle-cluster (PCA) structure, whereas for larger clusters CCA growth leads to more open or fluffy structures (Henning & Sablotny 1995). The code we use represents an exact calculation of the scattering matrix efficiencies of N clustered Rayleigh spheres touching but not interpenetrating each other. The results of this calculation for $N = 4$, $N = 16$, and $N = 32$ clusters are compared in Figure 3*b* with the extinction spectrum of a single sphere and with the spectrum of a

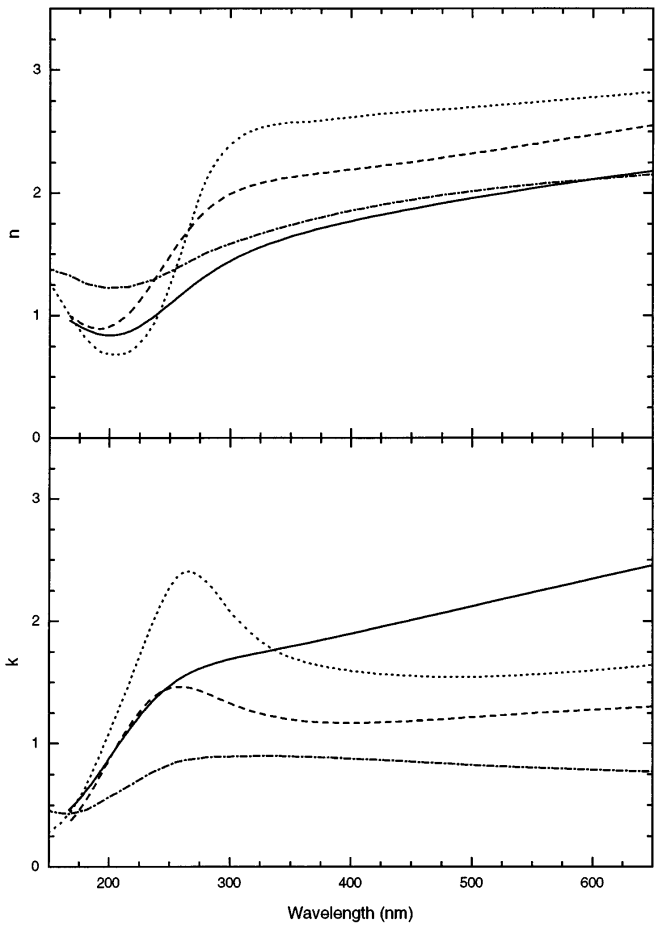

FIG. 4.—Optical data derived from the spectrum of isolated primary grains using a model with two Lorentz oscillators, assuming the sample to be a collection of perfect Rayleigh spheres. Plotted are *n* and *k* for the pure Argon sample (AR15; *solid line*) and for a hydrogenated sample (H50; *dashed line*). For comparison, the optical data for graphite (*dotted line*) reported by Draine & Lee (1984) and the recent data of Zubko et al. (1997) (*dash-dotted line*), derived from the clustered ACAR spectrum published by Colangeli et al. (1995) and plotted in Fig. 3, are also shown.

continuous distribution of ellipsoids (CDE), which is often used as an approximation for clustered samples.

The similarity of the measured UV spectra of the beam particles extracted at different distances (Fig. 3*a*) to the simulated spectra of the CCA aggregates is remarkable. A deviation occurs in the visible range, where the measured absorption decreases faster than the calculated curves. Here we should note that the scattering calculations for the CCA particles can only be a first approximation for the real optical behavior of the agglomerates, with their complicated structures. However, this deviation may also indicate some uncertainty in the optical data resulting from slight deviations of the actual grain shape from the sphere model. Indeed, further fitting iterations using somewhat more realistic spheroidal particle shapes have shown that a slight variation in the shape of the primary particles could account for the deviations in the long-wavelength region. However, in the UV hump region, the measured band broadening by an enhanced long-wavelength wing of the feature without an appreciable shift of the peak position is exactly reflected by the model calculations. This is a strong indication that the measured band broadening is indeed a result of the increase in particle clustering with increasing extraction distance, as proven by TEM analysis.

After the evaporation of the matrix (designated AR15RE in Fig. 3*a*), the UV feature of the AR15 sample is strongly broadened compared to the feature of the isolated sample, indicating a diffusion and coagulation of the particles during evaporation. The electron micrographs (Figs. 2*c* and 2*d*) show that the residue left on the substrate consists of strongly coagulated primary particles (Fig. 2*c*), which cover the whole substrate in a chainlike structure (Fig. 2*d*), similar to the morphological results reported for the ACAR particle sample (Colangeli et al. 1995). Therefore, the variation in the spectrum resulting from evaporation represents the spectral change in the absorption properties that can generally be expected after the isolated-nonisolated transition in carbon grain samples. This is supported by the striking similarity of the AR15RE spectrum to the ACAR spectrum (Fig. 3*a*).

A rough approximation of the shape distribution in such strongly clustered grain samples is given by a continuous distribution of ellipsoids (CDE; Huffman 1988). Indeed, the CDE calculation in Figure 3*b* reflects qualitatively the spectral behavior of the AR15RE experimental curve in Figure 3*a*. Nevertheless, there are still significant differences between the CDE and the AR15RE spectra not only for longer wavelengths but also in the hump region. In this respect, the optical data derived by Zubko et al. (1997) from the ACAR spectrum (which compares quite well to the AR15RE spectrum in Fig. 3*a*) using a CDE grain model can only be considered as a rough approximation of these quantities, at most.

Another, simpler approach to deriving the absorption characteristics of strongly coagulated grain samples is to use a thin porous layer, the dielectric function of which is described by an effective medium theory (EMT). This is also not without problems; EMTs are not exact at the resonances of the dielectric function, and the porosity in the layer is on a scale comparable with the wavelength. Nevertheless, for a reasonable volume filling factor of 25%, AR carbon and a Bruggeman-type model (Bruggeman 1935) reproduce exactly the CDE calculation. This shows that a number of simple models may give the correct general trend for clustering effects in the UV spectral behavior of carbon grain samples. Nevertheless, they are not suitable for determining optical constants from the spectra of such clustered samples.

The above results prove that the π-π^* absorption feature is influenced by surface modes, and therefore that morphological effects must be taken into account when discussing the extinction characteristics of (coagulated) carbon grains. Furthermore, as a result of these effects an exact modeling of the grain morphology in the sample is necessary to derive reliable optical data of the particle material, especially in the hump region.

3.2. *The Effect of Hydrogenation*

To investigate the effect of hydrogen incorporation on the π-π^* transition of the carbon network, a second set of samples was prepared, with varying hydrogen content in the quenching gas. The extraction distance in this run was 15 mm from the source, to ensure that the freshly condensed nanoparticles were extracted and isolated in a noncoagulated state. This was checked by TEM analysis, as in the samples before. The mixing ratio between hydrogen and argon in the quenching gas was successively enhanced from 1:100 to pure hydrogen for the individual samples, while the pressure was held constant at 10 mbar.

Fourier transform infrared spectroscopy of the distinct carbon materials was performed in the wavelength range from 2–20 μm. Such data are extremely important for the interpretation of ISO data. The measurements were done for both the beam particles and the material left in the condensation chamber. Quantitative spectroscopy leading to a quantitative determination of the incorporated hydrogen was only possible for the latter material. To that end, carbon particles were scraped from the extraction nozzle in the evaporation chamber and dispersed in KBr pellets.

The results of the quantitative evaluation of the carbon grain spectra are shown in Figure 5. First, there is a clear decrease in the continuum absorption as the hydrogen content in the quenching gas increases, except in the case of pure hydrogen, where the continuum slope is less steep (Fig. 5*a*). Second, the decrease in continuum absorption is correlated with a strengthening of the C-H vibrations (Fig. 5*b*). This indicates that an increasing amount of hydrogen is indeed incorporated into the carbon material when the hydrogen content of the quenching gas is increased. The pure hydrogen sample is an exception to that rule, pointing to a completely different condensation mechanism in this case. Furthermore, the ratio between the aromatic and the aliphatic site vibrations, located at 3.3 and 3.4 μm, respectively, remains quite constant, indicating that incorporation of the hydrogen in the carbon network is not selective. This, however, needs to be proven by an independent determination of the sp^2/sp^3 ratio.

From the integrated strength of the C-H bands, we determined quantitative values for the hydrogen content of the materials, following Jacob & Unger (1996) and using a value of $A^{-1} = 1.2 \times 10^{-21}$ cm^2 for the absorption cross section per C-H bond. The resulting values are tabulated in Table 1. Additional CHN microcombustion analysis confirmed the infrared results qualitatively, but gave significantly higher hydrogen contents (Table 1). This fact must be attributed to hydrogen and water physisorbed at the grain surface, which makes the microcombustion not suitable for quantitative investigation of the C/H network.

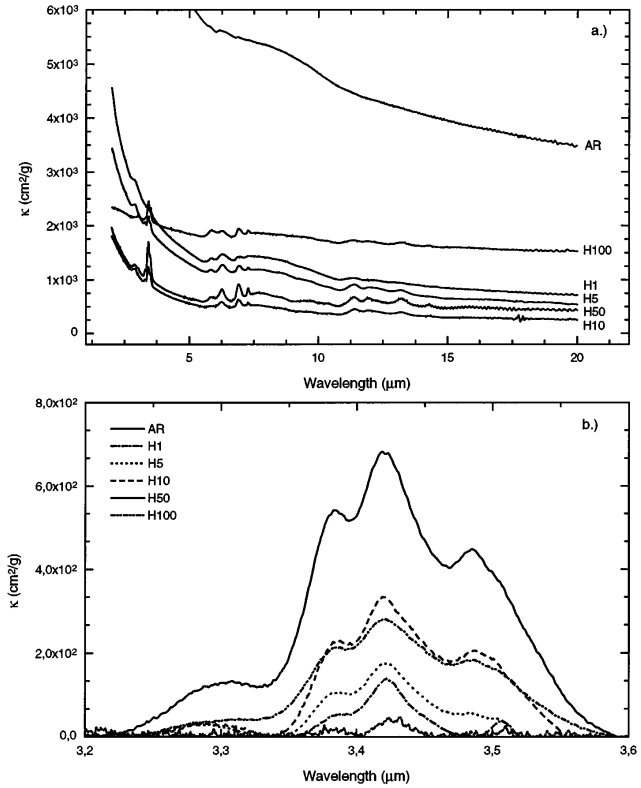

FIG. 5.—IR absorption spectra of carbon grains quenched at varying hydrogen contents and sampled in the source chamber. (*a*) Continuum absorption slope. (*b*) Spectral region of the C-H stretching vibrations after substraction of the continuum. Quenching gas composition is shown for pure Ar (AR15; *solid line*), H_2:Ar = 1:100 (H1; *dashed line*), H_2:Ar = 5:100 (H5; *dotted line*), H_2:Ar = 1:10 (H10; *dash-dotted line*), H_2:Ar = 5:10 (H50; *dash-double-dotted line*), and pure H_2 (H100; *short-dashed line*).

To get a qualitative comparison between the material from the condensation chamber and the beam particles, we also deposited carbon grains from the beam onto KBr substrates. The use of the microbalance was not possible in this case, so the deposited samples (masses $\leq$0.1 mg) could not be treated by quantitative spectroscopy. Therefore, the comparison of the IR results shown in Figure 6 is plotted in arbitrary absorbance units. The spectral representation in logarithmic units is useful for an easy comparison with the recent results of Herlin et al. (1997) for carbon nanoparticles produced by a laser-driven gas-phase pyrolysis of C_2H_4 and C_4H_6 precursors. The comparison of their IR spectra with recent ISO data observed in emission from planetary nebulae by Beintema et al. (1996) have brought hydrogenated solid carbon particles back into the discussion of the carrier of the unidentified infrared bonds (UIBs).

TABLE 1

HYDROGEN CONTENT IN THE QUENCHING GAS AND IN THE CARBON MATERIALS FROM CHN MICROCOMBUSTION AND IR ANALYSIS

Sample	Gas (%)	CHN (%)	IR (%)
AR	0.0	12.1	0.6
H1	1.1	24.3	4.3
H5	4.8	31.9	7.8
H10	9.1	35.3	17.3
H50	33.3	...	46.0
H100	100.0	34.0	20.6

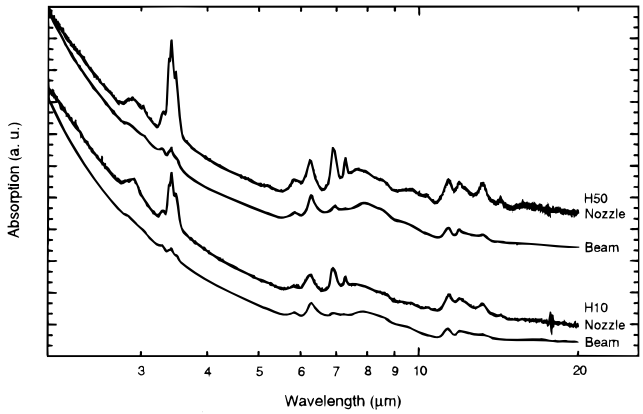

FIG. 6.—Comparison of the infrared spectra for the beam particles and the material from the condensation chamber ("nozzle") for two different values of the hydrogen content in the cooling gas.

The spectra of the carbon materials from the nozzle are relatively similar to the spectra obtained for the deposited beam particles (Fig. 6). However, there are deviations between the ratios of the C-H features around 3.4, 6.9, and 7.3 μm, assigned to aliphatic C sites and the C-H bands at 3.3 and from 11 to 14 μm, corresponding to aromatic C sites. This behavior indicates an enhanced aromatic character in the structure of the beam particles as compared to the carbon material taken from the condensation chamber.

The UV absorption spectra of the matrix-isolated samples in this series are plotted in Figure 7. The small periodic structure superimposed on some spectra at longer

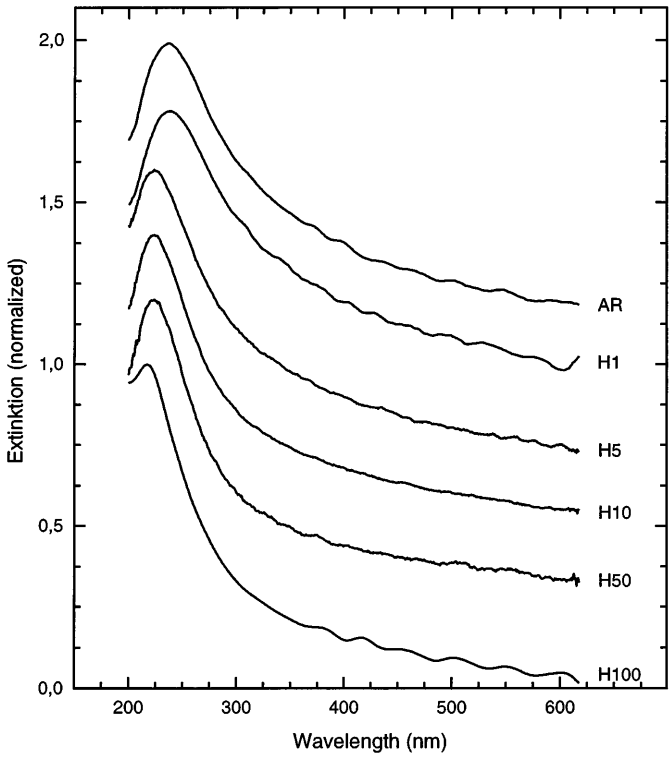

FIG. 7.—UV-VIS absorption spectra of isolated carbon grains extracted at 15 mm from the source in a quenching gas atmosphere at 10 mbar with varying hydrogen content. The offset between the spectra is 0.25. Shown, from top to bottom, are: pure Ar (AR15), H_2:Ar = 1:100 (H1), H_2:Ar = 5:100 (H5), H_2:Ar = 1:10 (H10), H_2:Ar = 5:10 (H50), and pure hydrogen (H100).

wavelengths is an interference pattern arising from small variations in the thickness between the sample and the reference matrix layer. The sample H1 prepared at 1 atom% hydrogen content still behaves like the pure argon sample within the resolution of the spectrometer. However, a large blueshift of about 13 nm (from 237 to 224 nm) is observed when the hydrogen content of the quenching gas is increased to 4.8 atom%. This shift is in general agreement with the results found for hydrogenated amorphous carbon particles and thin films. The blueshift is usually attributed to an increased sp^3 site content in this material, resulting in smaller and more separated graphite units.

Much more surprising is the fact that for higher hydrogen contents in the cooling gas the peak position remains stable, while the peak width slightly decreases. Only for the final big step in hydrogen content from 33 atom% in the H50 sample to 100 atom% in the H100 sample does the peak position get a further blueshift to a position of 217 nm. We should note that this may be the result of a strong change in the internal structure of the grains in the H100 sample. This suggestion is supported by a less steep continuum slope of the H100 spectrum (Fig. 5*a*), indicating an enhanced quantity of tail and defect states in the gap region of this material.

In the standard model of amorphous or disordered carbonaceous material, the UV absorption feature is attributed to π-π^* interband transitions in small units composed of plane graphitic sheets (Robertson & O'Reilly 1987). Following this model, the band structure is determined by the size distribution of these graphitic microislands, which can be monitored by analyzing the gap energy. The gap energy can be derived from the Tauc relation $E[\epsilon_2(E)]^{1/2} \sim E - E_g$ (Tauc, Grigorovici, & Vancu 1966), where $E = \hbar\omega$ is the photon energy, $\epsilon_2 = 2nk$ is the imaginary part of the dielectric function, and E_g is the gap energy of the material. This relation is often used to derive E_g directly from the absorption spectra $\alpha(E)$ measured on compact thin films, where $\alpha(E) \sim E\epsilon_2$ is valid in the case of $n \approx$ const. We should note that this procedure is sometimes misused to derive E_g from the absorption spectra of particle samples, where $\alpha(E) \sim E\epsilon_2$ is not valid.

Hydrogen incorporation has been supposed to trigger a decrease in crystallite size. This is supported by annealing experiments on thin films, starting with a hydrogenated sp^3-dominated carbonaceous material and observing the crystallite growth by analyzing the gap energy decrease (Koidl et al. 1989). However, according to new results found by Paret et al. (1997) for freshly deposited CVD carbon films, a tight correlation of the gap energy with the hydrogen content is not found.

The derivation of the optical data from the spectra of the AR and H50 particles in the previous section enables us to determine the gap energy of the grain material based directly on ϵ_2. The analysis showed that the gap energy E_g is zero for both materials. This points to a highly graphitic structure (many large graphitic units in the framework of the Robertson model), even for particles produced in the hydrogen-containing atmospheres. This result is consistent with both the graphite-like optical data (cf. Fig. 4) and the relatively weak aliphatic C-H bands observed for the beam particles (Fig. 5).

In annealing experiments on hydrogenated carbon grains deposited on a substrate, a correlation between the gap energy and the UV feature position was found (Mennella et al. 1995b). Our results definitely do not fit this correlation, since for their zero-gap samples a peak position of larger than 250 nm was found. There are several possible explanations for this discrepancy. First, it may be partly a consequence of the clustering present in their samples. Second, the form of the Tauc relation used by Mennella et al. (1995b) is only valid for compact thin films. Finally, the correlation may not be valid at all for the kind of carbon network produced in our experiments.

We should note that not only the crystallite size but also the arrangement of the crystallites influence the optical properties (Michel et al. 1998). Carbon particles produced in hydrogen-containing atmospheres are known to show (apart from disorderly arranged graphitic units) onionlike structures consisting of concentrically arranged graphitic sheets (Jäger et al. 1998; Harris et al. 1994). The decrease in the UV feature width shown in Figure 7 and the steeply decreasing IR continuum slope suggest that there might be an enhanced structural order present in the grains of these samples. All these suggestions concerning the internal structure will be the subject of further investigations by high-resolution TEM and electron energy-loss spectroscopy (EELS).

4. ASTROPHYSICAL CONSIDERATIONS

4.1. *Comparison with the 217.5 nm Hump Profile*

According to equation (1), the interstellar extinction curve can be parameterized in the hump region by a linear background plus a Drude profile. Besides the hump carrier, other components of the interstellar dust also contribute to the linear background. To enable a quantitative comparison between the observed hump profile and our spectroscopic results for matrix-isolated grains, we applied the same parameterization scheme to the latter and compare only the derived Drude profile parameters (strength a_3/γ^2, peak position λ_0^{-1}, and width γ).

Table 2 gives the parameterization results for the pure and hydrogenated isolated carbon grain samples; the profile becomes narrower and blueshifted in peak position compared to the pure argon sample when hydrogen is incorporated effectively, or, more precisely, when the hydrogen content in the quenching gas is $\geq 5\%$. No correlation of the profile strength with the quenching-gas composition was found, even if the variation of the values is enhanced. Furthermore, Table 2 shows that the fits are improved with

TABLE 2

RESULTS OF DRUDE PROFILE FITS FOR MATRIX-ISOLATED SINGLE NANO-SIZED CARBON GRAINS

Sample	$a_3\gamma^2$ (10^5 cm^2 g^{-2})	λ_0^{-1} (μm^{-1})	γ (μm^{-1})	χ^2 (10^6)
AR	2.499	4.09	1.83	131
	2.137[a]	4.46[a]	1.48[a]	4.73[a]
H1	2.750	4.12	2.40	109
H5	1.824	4.33	1.32	14.7
H10	2.044	4.38	1.24	8.31
H50	2.606	4.42	1.35	6.32
	2.392[a]	4.68[a]	1.42[a]	2.23[a]
H100.....	3.381	4.61	1.59	11.5
ISM[b].....	...	4.60 ± 0.04	0.99 ± 0.25	...

NOTE.—The parameters of the mean interstellar hump profile represent the observational constraints.

[a] In vacuum.

[b] Average values reported by Fitzpatrick & Massa 1986.

increasing hydrogen content from the pure argon case up to a quenching-gas composition of $Ar:H_2 = 100:50$, corresponding to a hydrogen content of $\sim 33\%$. To take matrix-induced effects into consideration, the Drude parameters for the spectra of Rayleigh spheres in vacuum calculated from the optical data compiled in § 3 for the AR15 and H50 spectrum are given in parenthesis. For the sample produced in a pure hydrogen atmosphere, the fit gets slightly worse again.

To illustrate the quality of the applied parameterization procedure and the relevance of these results to astrophysics, the decomposition of the best-fitting H50 spectrum is shown in Figure 8*a*. The normalized Drude profile of the matrix-corrected H50 spectrum is compared with the corresponding profile of the mean interstellar extinction curve in Figure 8*b*. We stress that this is the best fit of the 217.5 nm hump ever published for real carbonaceous dust analogs.

4.2. *Elemental Abundance Constraints*

Apart from observational constraints, elemental abundance constraints are also important tools for assessing the astrophysical relevance of dust models. Owing to new determinations of the cosmic carbon abundance by NLTE analysis of B star atmospheres, the cosmic carbon budget has been drastically revised in the past few years (for a discussion see Snow & Witt 1995; Henning 1997). The widely adopted solar value is now considered to be too large. In connection with the new determinations of gas-phase abundances in the diffuse interstellar medium by the Goddard High Resolution Spectrograph aboard the *Hubble Space Telescope*, tighter limits have resulted for the amount of carbon locked in solid dust particles (Cardelli et al. 1996).

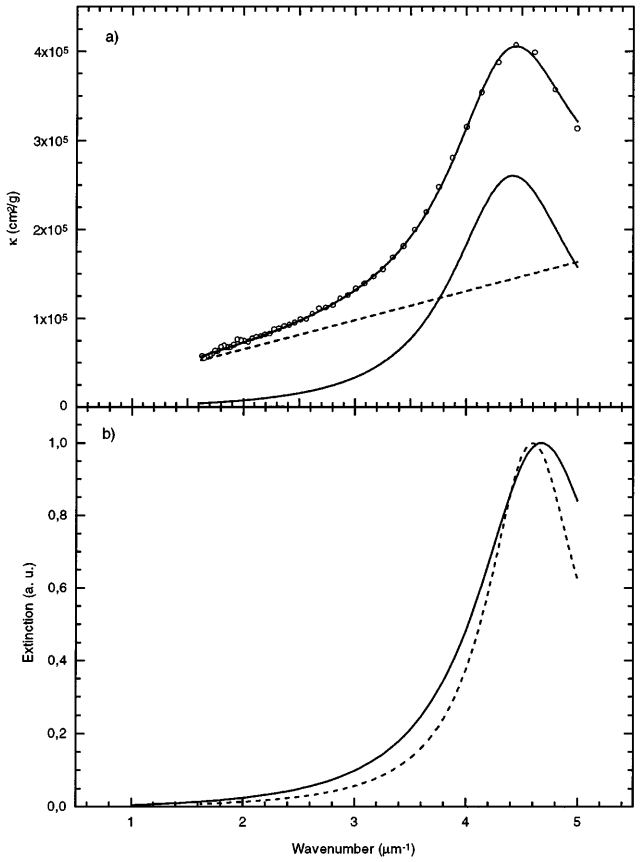

FIG. 8.—(*a*) Decomposition of the H50 sample spectrum (*open circles*) in a linear component (*dashed line*) and a Drude profile (*solid line*). (*b*) Comparison of the matrix-corrected H50 profile (*solid line*) with the Drude component of the mean interstellar extinction curve (*dashed line*).

As mentioned in the previous section, the 217.5 nm hump of the interstellar extinction curve is superimposed on a continuum extinction caused by other dust components as well as by the hump carrier itself. Therefore, in order to estimate the amount of carbon required in the interstellar medium for our analog samples, the extinction values of the Drude parts evaluated from the absorption spectra should be compared with the strength of the 217.5 nm hump profile. The normalized extinction strength of the mean ISM Drude profile, $(a_3/\gamma^2)_{\rm ISM}/E_{B-V} = 3.32$, given by Fitzpatrick & Massa (1986), can be converted into an extinction cross section per 10^{21} hydrogen atoms by using the ratio between the column density of elemental hydrogen $N_{\rm H}$ and the color excess E_{B-V}, for which $N_{\rm H}/E_{B-V} = 5.9 \times 10^{21}$ cm^{-2} is usually taken (Bohlin, Savage, & Drake 1978). With these values, we get $(a_3/\gamma^2)_{\rm ISM}/10^{21}N_{\rm H} = 0.562$ cm^2 for the extinction cross section in the profile maximum. The requirement that this value be caused by our analog material fixes the required carbon abundance at

$$\frac{(a_3/\gamma^2)_{\rm ISM}}{10^{21}N_{\rm H}} = \frac{N_{\rm C}}{10^{21}N_{\rm H}}\, 12m_{\rm H}\left(\frac{a_3}{\gamma^2}\right)_{\rm sample}, \qquad (2)$$

where $N_{\rm C}$ is the required carbon column density, $m_{\rm H} = 1.66 \times 10^{-24}$ g is the mass of the hydrogen atom, and $(a_3/\gamma^2)_{\rm sample}$ is the profile strength of our samples tabulated in Table 2. The results of this estimate for the different grain samples are compared in Table 3 with the latest elemental abundance constraints found in the literature. A carbon abundance per million hydrogen atoms (ppm) of ~ 115 is required to be locked in the hump carrier for our analog samples. This value is less than the available solid carbon amount of ~ 215 ppm that remains when the solar carbon abundance is assumed as reference and the amount present in the gas phase is subtracted. Thus, the assumption that isolated nano-sized carbon particles could account for the 217.5 nm hump in the interstellar medium extinction curve cannot be ruled out by cosmic carbon abundance considerations when using the solar value as reference. Apparently, our analogs encounter some problems when the new cosmic abundance determinations for young objects (stars and nebula) are adopted as a reference. In this case, a fractional

TABLE 3

REQUIRED CARBON ABUNDANCES FOR ISOLATED GRAIN SAMPLES CONSTRAINED BY HUMP STRENGTH OF MEAN INTERSTELLAR EXTINCTION CURVE

Sample	C/H (10^{-6})	Notes
AR	113	
	130	in vacuum
H1	103	
H5	155	
H10	138	
H50	108	
	118	in vacuum
H100	84	
Solar	355 ± 50	Grevesse & Noels (1993)
Cosmic (young objects)	225 ± 50	Snow & Witt (1995)
Interstellar gas	140 ± 20	Cardelli et al. (1996)

NOTE.—For comparison, the latest determinations of the carbon abundance constraints are given.

amount of only ~ 85 ppm carbon atoms are left to form solid particles; only the H100 sample slightly underbids this narrow abundance span. However, it should be noted that there may still be systematic errors in these abundance derivations, and that the heavy elements may not be completely incorporated into stars during massive star formation.

4.3. *Implications for Dust Models*

As we have shown in the last two sections, the Drude component derived from the mean interstellar extinction curve in the hump region can be represented quite well in terms of the observational and abundance constraints by Drude profiles of extinction measurements performed on isolated small (hydrogenated) carbon grains. On the other hand, the overall observed interstellar extinction curve is a superposition of extinction contributions from different dust components with distinct physical properties (material, size, shape, etc.). Therefore, it is interesting to see what part of the interstellar extinction curve is left when we assume our analog to be responsible for the Drude part of the hump. Thus, according to equation (2), the mass extinction coefficient spectra of the samples must be scaled by $10^{-21} 12 m_{\rm H}({\rm C/H})_{\rm sample}$ to get the extinction curve per 10^{21} hydrogen atoms attributed to the analog particles. In Figure 9, the resulting extinction spectrum for the matrix-corrected H50 sample [$({\rm C/H})_{\rm H50} = 118$ppm] is compared with the mean interstellar extinction curve. To indicate the part of the interstellar extinction curve that is due to other dust components, the difference between them is also plotted. This compares favorably to the extinction curve calculated for core mantle particles formed from a silicate core and an organic refractory mantle in the dust model proposed by Li & Greenberg (1997). Indeed, in this model the component attributed to the hump profile is a separate grain population with the absorption strength of small graphite particles but no further specifications. An abundance of 37.4 ppm carbon is required for this population by the authors. Furthermore, a carbon abundance of 108 ppm is required to be locked up in the organic refractory mantles of the larger particles responsible for the wavelength-dependent extinction in the infrared and visible and the neutral extinction in the ultraviolet. Compared to these abundance values, the core-mantle particle amount can be reduced by $\sim 10\%$, leading to a carbon abundance of ~ 97 ppm locked up in the mantles when the hump is attributed to the H50 grains. This is due to a higher absorption level in the visible spectral region for the real H50 grains as compared to the visible absorption of hump grains included in the model. On the other hand, the lower absorption strength of the H50 grains compared to the strength calculated for graphite spheres leads to an enhanced carbon abundance of 118 ppm for these grains (see Table 3). Thus, the total carbon abundance for a modified dust model composed of core mantle plus H50 particles (as the hump carrier) is calculated to be ~ 215 ppm, clearly more than the 145 ppm required for the unmodified model. Here one has to take into account that a further carbon abundance of ~ 49 ppm is required for the far-UV rise in this unmodified model, which also contributes to the extinction in the hump region. This far-UV rise is attributed to absorption by PAHs by the authors, but based only on the absorption strengths and not on the spectral characteristics of analog samples measured in the laboratory. Furthermore, our analog samples will certainly contribute to this far-UV rise because of strong σ-σ^* transitions located at around 80 nm, as detected by EELS analysis (Jäger et al. 1998). Taking this into account, the total required carbon amount of ~ 215 ppm for our model formed of core-mantle plus H50 particles is comparable to the total amount of ~ 194 ppm for the three-component model (core mantle, hump, and PAH) of Li & Greenberg (1997).

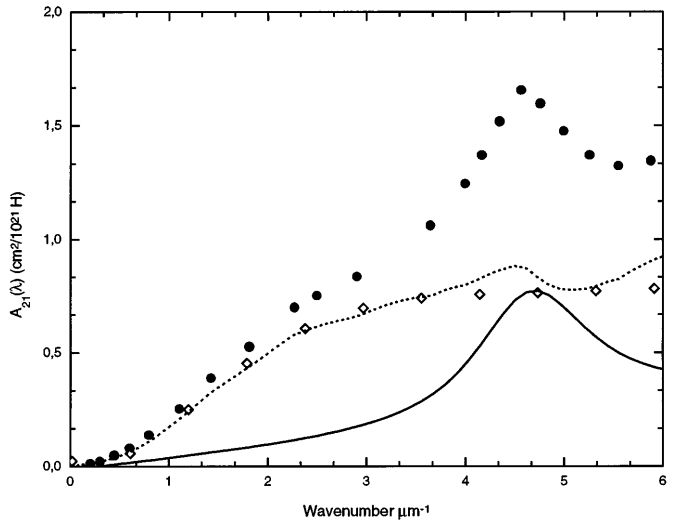

FIG. 9.—Mean interstellar extinction curve (*solid circles*) compared with the matrix-corrected H50 spectrum (*solid line*), which is scaled in such a way that the Drude part of this spectrum completely accounts for the corresponding Drude part of the interstellar extinction. The difference between them (*dashed line*) represents the part of the extinction curve that can be attributed to other dust components. This difference compares quite well to the extinction curve calculated for core-mantle particles by Li & Greenberg (1997) (*diamonds*).

The present comparisons of our results with observations, abundances, and dust models have shown that the isolated nano-sized carbon grains could serve as a real dust analog for the carrier of the 217.5 nm hump of the interstellar extinction curve, and that they therefore should be included in further, more realistic dust models for the interstellar medium dust.

5. SUMMARY AND CONCLUSIONS

In this paper we have shown that particle shape and clustering strongly influence the absorption characteristics of small carbon particles. The effects of clustering and hydrogenation on UV-VIS spectral behavior could be investigated separately by matrix isolation. In any case, a narrowing of the π-π^* feature was found for the isolated grain samples as compared to the coagulated carbon grain samples investigated so far in the laboratory.

Small changes in the clustering state affect mainly the feature width and less the peak position, in agreement with theoretical investigations of compact particle clusters.

Above a certain lower limit of hydrogen content in the quenching gas, hydrogen is incorporated into the atomic structure of the carbon grains. The corresponding change in the internal bonding structure results in a blueshift of the UV feature toward a peak position of 224 nm, which is comparable (after the correction of the matrix shift) to the position of the 217.5 nm hump in the interstellar extinction curve. Further changes in the hydrogen content of the cooling gas also result mainly in a change of the UV feature width, while the peak position remains quite stable.

We also present infrared spectra of the hydrogenated carbon samples and discuss the incorporation of hydrogen into the carbon network. These data should be extremely helpful for the interpretation of ISO results.

We thank H.-W. Meyer and his staff at the Institut für Ultrastrukturforschung Jena for providing the TEM and for their help in operating it. This work has been supported by the Deutsche Forschungsgemeinschaft (DFG grant Mu 1164/1-1). H. M. is supported by a grant from the Max Planck Society to Th. H. The collaboration between Th. H. and F. S. was supported by a grant through the German-American Research Networking program.

REFERENCES

Andrews, L., & Moskovits, M. 1989, in Chemistry and Physics of Matrix-Isolated Species, ed. L. Andrews & M. Moskovits (New York: Elsevier), 1
Barnes, A. J. 1981, in Matrix Isolation Spectroscopy, ed. A. J. Barnes, W. J. Orville-Thomas, A. Müller, & R. Gaufrés (NATO ASI Series C) (Dordrecht: Reidel), 13
Beintema, D. A., et al. 1996, A&A, 315, L369
Bohlin, R. C., Savage, B. D., & Drake, J. F. 1978, ApJ, 224, 132
Bohren, C. F., & Huffman, D. R. 1983, Absorption and Scattering of Light by Small Particles (New York: Wiley)
Bruggeman, D. A. G. 1935, Ann. Phys. (Leipzig), 24, 636
Cardelli, J. A., Clayton, G., & Mathis, J. 1989, ApJ, 345, 245
Cardelli, J. A., Meyer, D. M., Jura, M., & Savage, D. 1996, ApJ, 467, 334
Colangeli, L., Mennella, V., Palumbo, P., Rotundi, A., & Bussoletti, E. 1995, A&AS, 113, 561
Dorschner, J. 1973, Ap&SS, 25, 405
Draine, B. T., & Lee, H. M. 1984, ApJ, 285, 89
Edoh, O. 1983, Ph.D. thesis, Univ. Arizona
Fitzpatrick, E. L., & Massa, D. 1986, ApJ, 307, 286
Grevesse, N., & Noels, A. 1993, in Origin and Evolution of the Elements, ed. N. Prantzos, E. Vangioni-Flam, & M. Cassé (Cambridge: Cambridge Univ. Press), 15
Harris, P. J. F., Tsang, S. C., Claridge, J. B., & Green, M. L. H. 1994, J. Chem. Soc. Faraday Trans., 90, 2799
Henning, Th. 1997, in IAU Symp. 178, Molecules in Astrophysics, ed. E. van Dishoeck (Dordrecht: Kluwer), 343
Henning, Th., & Sablotny, R. 1995, Adv. Space Res., 16(2), 17
Herlin, N., Bohn, I., Reynaud, C., Cauchetier, M., Galvez, A., & Rouzaud, J.-N. 1997, A&A, in press
Hong, S. S., & Greenberg, J. M. 1980, A&A, 88, 194
Huffman, D. R. 1988, in Experiments on Cosmic Dust Analogues, ed. E. Bussoletti, C. Fusco, & G. Longo (Dordrecht: Kluwer), 345
Jacob, W., & Unger, M. 1996, Appl. Phys. Lett., 68, 475
Jäger, C., Henning, Th., Spillecke, O., & Schlögl, R. 1998, in preparation
Jenniskens, P., & Greenberg, J. M. 1993, A&A, 274, 439
Koidl, P., Wild, Ch., Dischler, B., Wagner, J., & Ramsteiner, M. 1989, in Properties and Characterization of Amorphous Carbon Films, ed. J. J. Pouch & S. A. Alterovitz (Zürich: Trans Tech), 41
Li, A., & Greenberg, J. M. 1997, A&A, 323, 566
Mathis, J. S. 1996, ApJ, 472, 643
Mathis, J. S., Rumpl, W., & Nordsieck, K. H. 1977, ApJ, 217, 425
Mennella, V., Colangeli, L., Blanco, A., Bussoletti, E., Fonti, S., Palumbo, P., & Mertins, H. C. 1995a, ApJ, 444, 288
Mennella, V., Colangeli, L., Bussoletti, E., Monaco, G., Palumbo, P., & Rotundi, A. 1995b, ApJS, 100, 149
Michel, B., Henning, Th., Jaeger, C., & Kreibig, U. 1998, in preparation
Papoular, R., Conard, J., Guillois, O., Nenner, I., Reynaud, C., & Rouzaud, J.-N. 1996, A&A, 315, 222
Paret, V., et al. 1997, J. Non-Cryst. Solids, in press
Preibisch, Th., Ossenkopf, V., Yorke, H. W., & Henning, Th. 1993, A&A, 279, 577
Robertson, J., & O'Reilly, E. 1987, Phys. Rev. B, 35, 2946
Rouleau, F. 1996, A&A, 310, 686
Rouleau, F., Henning, Th., & Stognienko, R. 1997, A&A, 322, 633
Rouleau, F., & Martin, P. G. 1991, ApJ, 377, 526
Savage, B. D. 1975, ApJ, 270, 169
Schnaiter, M., Mutschke, H., Henning, Th., Lindackers, D., Strecker, M., & Roth, P. 1996, ApJ, 464, L187
Schulze, W., & Kolb, D. M. 1973, J. Chem. Soc. Faraday Trans. II, 70, 1098
Snow, T. P., & Witt, A. N. 1995, Science, 270, 1455
Stecher, T. P. 1965, ApJ, 142, 1683
Stognienko, R., Henning, Th., & Ossenkopf, R. 1995, A&A, 296, 797
Tauc, J., Grigorovici, R., & Vancu, A. 1966, Phys. Status Solidi, 15, 627
Zubko, V. G., Mennella, V., Colangeli, L., & Bussoletti, E. 1997, MNRAS, 282, 1321